Instrument Science Report WFC3 2019-04

Time-dependent WFC3/IR Superdarks

Ben Sunnquist, Myles Mckay & Sylvia Baggett

May 1, 2019

Abstract

We create new WFC3/IR dark calibration files for all allowed observing modes. Unlike previous superdark releases, we update the values of any time-dependent pixels in these new superdarks on a cycle-by-cycle basis, which allows for better calibration of those ∼3.5% of detector pixels that have changed their dark current behavior since launch. These new superdarks also incorporate an additional four years of dark calibration data since the previous release, which reduces the errors associated with the superdark values by 8.9-67% depending on the observing mode. These new superdarks have been delivered and incorporated into the calwf3 pipeline along with the new accompanying time-dependent WFC3/IR bad pixel tables (Sunnquist et al., 2019). For drizzled data products, a new AstroDrizzle parameter table should be used together with these new reference files in order to recover the stable hot pixels (Mack & Bajaj, 2019).

1 Introduction

WFC3/IR images taken with no light source present on the detector (i.e. images taken with an aluminum blank in the light path) show an underlying dark current signal induced by the detector's internal thermal background. The `calwf3` pipeline removes this signal by subtracting a superdark (a combination of many individual dark exposures) from each individual WFC3/IR image.

While the detector-wide dark current levels have remained stable at ∼0.021 DN/s (0.049 e^-/s) since launch (Sunnquist et al., 2017-04; Hilbert & Petro, 2012), ∼3.5% of the detector pixels have shown an evolution in their dark current behavior over this same time period (Sunnquist et al., 2019; Figure 1). In this report, we generate new WFC3/IR superdarks that incorporate an extra four years of data acquired since the previous superdark release

(Dulude et al., 2014-06). Unlike past releases, we also update these new superdarks each cycle in order to more accurately reflect the observed behavior changes of those time-dependent detector pixels.

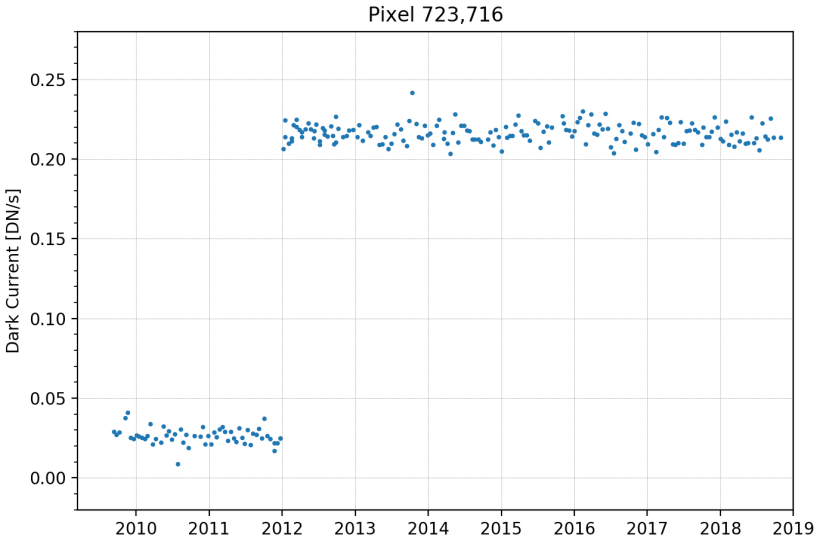

Figure 1: A pixel that becomes hot after exhibiting a normal dark current level.

2 Data

We use darks from the internal WFC3/IR dark monitoring programs to generate the time-dependent superdarks. These monitoring programs are executed each cycle and obtain multiple darks for every observing mode (i.e. every sample sequence and aperture combination) offered to external users. The total number of darks obtained in each observing mode is dependent on the popularity and newness of the mode. Other than the full-frame SPARS200 darks, which are taken regularly ∼every two weeks to monitor the bad pixel populations, the darks are generally allowed to be taken any time throughout the cycle in these proposals; this relaxed scheduling is possible due to the stability of the overall dark current level. Table 2 in Section 3 shows the WFC3/IR dark monitoring program number belonging to each cycle.

We run each of the individual `RAW` dark exposures through the `calwf3` pipeline (Version 3.4) to obtain calibrated `IMA` files. We generate the superdarks using these `IMA` files since the `calwf3` pipeline subtracts the dark current on a read-by-read basis. We run the pipeline with the following switches turned on: `DQICORR` (data quality initialization), `ZOFFCORR` (zero read subtraction), `BLEVCORR` (reference pixel correction), `NLINCORR` (non-linearity correction), `CRCORR` (cosmic ray detection), `UNITCORR` (count rate conversion).

We obtain the corresponding persistence products for the dark exposures from the MAST archive (`https://archive.stsci.edu/prepds/persist/search.php`); these products provide an estimate of the persistence levels in an exposure due to IR observations taken up to 16 hours prior to the exposure. Using these products, we flag any pixels in the dark exposures whose persistence levels are estimated to be greater than 0.002 DN/s (0.005 e^-/s, or ∼10% of the median dark rate (Sunnquist et al., 2017-04)) and exclude them during the

creation of the time-dependent superdarks. Details on IR persistence and a description of the model can be found in Long et al. (2015).

In addition to persistence, we also reject any darks that exhibit banding - an effect that leaves a rectangular region across an image that has a higher or lower signal than the rest of the image (Dulude et al., 2011). Banding mainly affects darks from the earliest dark monitoring programs - before the effect and its prevention were well understood.

In Table 1, we show the number of input files used to generate the old superdarks compared to the new superdarks presented in this report. As we'll explain in Section 3, we use data up to Cycle 25 to generate the superdark values for the time-dependent pixels, but only use up to Cycle 24 for the static pixels (i.e. those pixels with a stable dark current), which is what is represented in this table.

Table 1: The number of input images used to generate the old and new superdark for each observing mode. The difference (in terms of exposure time) between these two numbers is shown in the final column. These numbers refer to the static pixels only (∼96.5% of the detector), as the number of images used to determine the superdark values for the time-dependent pixels varies (see Section 3). With the exception of the SPARS5 modes, the old superdarks here refer to those presented in Dulude et al. (2014-06). The old SPARS5 mode superdarks refer to those that were used by the `calwf3` pipeline before the delivery of the new superdarks presented in this report.

Sample Sequence	Aperture	# Old	# New	Difference (minutes)
SPARS200	IR	44	142	4578.13
SPARS100	IR	186	218	748.23
SPARS50	IR	195	241	538.92
SPARS25	IR	124	172	282.35
SPARS25	IRSUB512	42	80	203.78
SPARS25	IRSUB256	50	120	365.31
SPARS10	IR	69	135	157.24
SPARS10	IRSUB256	42	376	574.08
SPARS10	IRSUB128	62	171	182.85
SPARS5	IR	10	14	4.86
SPARS5	IRSUB512	12	29	11.83
SPARS5	IRSUB256	16	31	8.28
STEP400	IR	11	50	1819.51
STEP200	IR	109	154	1199.42
STEP100	IR	69	110	614.48
STEP50	IR	96	133	307.86
STEP25	IR	62	118	255.95
STEP25	IRSUB512	41	80	157.98
RAPID	IR	60	138	57.18
RAPID	IRSUB512	50	190	29.86
RAPID	IRSUB256	127	213	5.97
RAPID	IRSUB128	91	234	4.03
RAPID	IRSUB64	142	251	1.66

3 The Time-dependent Superdarks

Every cycle, we create new superdarks for each observing mode - treating the static and time-dependent pixels separately. Using the cycle-based bad pixel tables from Sunnquist et al. (2019), we identify pixels that have been historically hot or unstable (i.e. pixels that may exhibit a time-dependence in their dark current signals) and which have not (i.e. static pixels). In all of the superdarks, the values of the static pixels (∼96.5% of the detector) are determined by creating a full-stack of all of the dark data from cycles 17 to 24; because these pixels have a stable dark current over time, there is no need to treat each cycle independently. We do, however, analyze the dark current behavior of the potentially time-dependent pixels across each cycle, which allows us to determine which cycle's data to combine together to generate their superdark values in each cycle. By treating these two types of pixel populations this way, we ensure more accurate superdark values for the time-dependent pixels from cycle-to-cycle while still maximizing the number of darks used to determine the superdark values for the static pixels.

We zero-out all of the DQ arrays in these new superdarks in order to maximize the usefulness of the new time-dependent bad pixel tables from Sunnquist et al. (2019). If we did not perform this, the bad pixel flagging that is performed during the full-stack superdark generation process (Section 3.1) would be carried over during `calwf3` processing, and since these superdark DQ values are generated based on the full-stack, they would negate the time-dependence represented in the new bad pixel tables. We do, however, flag as unstable any time-dependent pixels that do not have enough data for their superdark values to be updated (see Section 3.2).

Since the creation of the full-stack values for the static pixels, an additional dark monitor proposal completed (Proposal 14986, Cycle 25). We opt to include the darks from this new proposal in our time-dependent step, but do not use them to re-create the full-stack values for the static pixels. Since we already have a large sample size for most observing modes (see Table 1), the effects of including an additional cycle's darks in this stack would be minimal.

We use the exposure start time of the first full-frame SPARS200 dark in each monitoring program as the USEAFTER date in each cycle's superdarks; this matches the USEAFTER dates used for the accompanying cycle-based bad pixel tables from Sunnquist et al. (2019). An exception to this are the Cycle 17 superdarks, which have an earlier USEAFTER of May 20, 2009 in order to calibrate all of the earliest WFC3/IR data. Also, we use August 31, 2015 as the USEAFTER for the Cycle 23 SPARS5 (a newly introduced sample sequence at the time) superdarks to ensure all of the earliest WFC3/IR SPARS5 data was calibrated and to match the old SPARS5 superdarks they were replacing.

Table 2: The corresponding WFC3/IR dark monitoring proposal for each cycle and the USEAFTER times for each cycle's superdarks. These times are used by the `calwf3` pipeline to ensure that the data from the different cycles are calibrated with the appropriate superdark.

Cycle	Proposal	USEAFTER	USEAFTER (MJD)
17	11929	May 20 2009 00:00:00	54971.00000000
18	12349	Nov 01 2010 22:08:59	55501.92290509
19	12695	Nov 02 2011 19:00:44	55867.79217593

20	13077	Nov 01 2012 06:04:35	56232.25318287
21	13562	Oct 21 2013 07:10:39	56586.29906250
22	14008	Oct 24 2014 22:38:39	56954.94350694
23	14374	Nov 03 2015 08:23:25	57329.34959491
24	14537	Oct 08 2016 15:00:50	57669.62557870
25	14986	Oct 02 2017 04:11:11	58028.17443287

3.1 Static Pixels

The large majority of pixels on the WFC3/IR detector (∼96.5%) have exhibited consistent dark current behaviors since launch (Sunnquist et al., 2019; Figure 2). To generate the values for these pixels in each cycle's superdarks, we follow the procedure outlined in Dulude et al. (2014-02), which essentially, after a rigorous dark vetting process, averages the values in all of the individual dark exposures together to create a full-stack superdark for each observing mode. Because these pixels show no time-dependence in their dark current levels, we can combine all of the data from every cycle together to generate these values in each cycle's superdarks (i.e. each cycle's superdarks will incorporate darks from every other cycle); this allows us to maximize the number of darks going into each of these measurements which minimizes the associated errors. As mentioned in Section 2, we use the calibrated `IMA` files to generate these full-stack superdarks (the `calwf3` pipeline subtracts the dark current read-by-read), and we exclude any pixels with estimated persistence levels greater than ∼10% of the overall median dark current level.

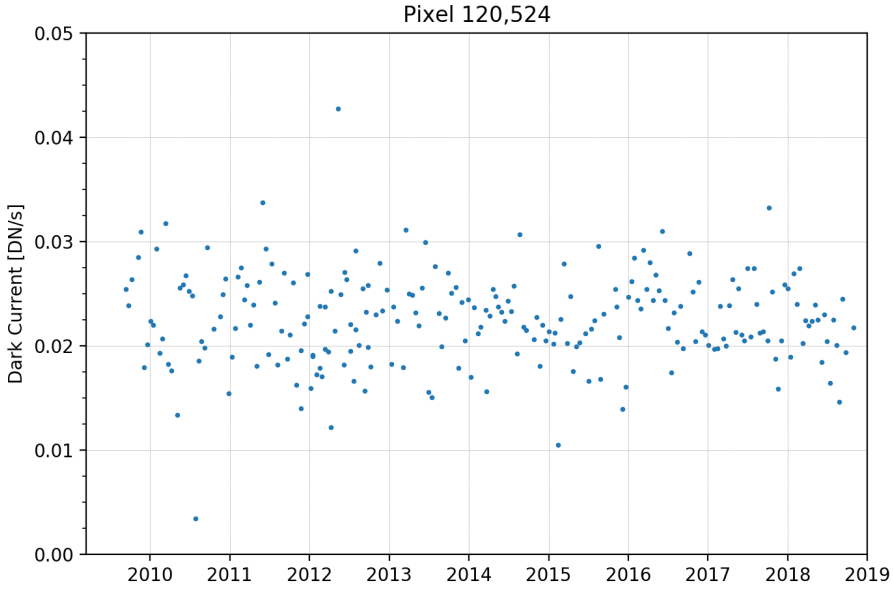

Figure 2: A pixel that has exhibited a normal (static) dark current level since launch.

After flagging the darks for persistence, we begin the dark vetting process to decide which darks to include in the full superdark stacks. First, we visually inspect the `IMA` science extensions and reject any darks with obvious anomalies (e.g. banding, scattered

light). Next, we observe the mean row and column values across each dark, and reject any darks where these distributions are significantly different from the rest. We then compare the mean values of each read for all of the darks, and reject any darks with abnormal up-the-ramp values compared to the rest. We also reject any darks that are significantly more faint or dark than the other darks for a given read.

After rejecting all of the darks that exhibit any of the anomalous behavior described above, we combine the remaining darks together to create a full-stack superdark for each observing mode. We generate these superdarks for each observing mode on a read-by-read basis by calculating the 3-sigma clipped robust mean of each pixel value through the vetted dark stack. Pixels flagged as bad (e.g. cosmic rays) are not included in these calculations. The corresponding error values for these pixels are the robust standard deviation of the values that went into the science average divided by the square root of the number of values used, and the corresponding sample values are the number of values used in these science and error calculations.

With the full-stack superdarks for each observing mode complete, we next visually and statistically inspect each extension to verify that the values are reasonable and that they represent the individual darks that went into their creation. We also compare the differences and distributions of each read to the previous superdarks from Dulude et al. (2014-06). Finally, we certify that these new superdarks contain the correct header information and that they run successfully as a dark reference file through the `calwf3` calibration pipeline.

These new full-stack superdarks are ideal for calibrating the static pixels, as they combine together all of the dark calibration data since launch. However, they are not ideal for any pixels with a time-dependent dark current level, as their values in these full-stack superdarks may be a combination of many different dark current behaviors. For this reason, we next modify the values of the pixels with a time-dependent dark current on a cycle-by-cycle basis in these new full-stack superdarks.

3.2 Time-dependent Pixels

Sunnquist et al. (2019) found that ∼3.5% of WFC3/IR pixels have changed their behavior since launch. In general, they found that the number of hot pixels (pixels with abnormally high dark current levels) grew by ∼200 pixels per cycle and the number of unstable pixels (pixels whose dark current levels show strong variations from image to image) could change by up to ∼4000 pixels per cycle; they also noted the existence of pixels becoming good, such as a pixel whose dark current stabilizes after years of instability or a hot pixel eventually dropping to a normal dark current level. Other pixel populations, however, such as bad-in-zeroth-read or dead pixels, did not show any changes in their numbers or locations over time. Due to these findings, we opt to modify the values of all historically hot and unstable pixels (i.e. any pixels that have ever been flagged as hot or unstable in any of the time-dependent bad pixel tables from Sunnquist et al. (2019)) on a cycle-by-cycle basis in the full-stack superdarks generated in the previous section. Of course, not all of these pixels exhibit a time-dependent dark current (e.g. a pixel that has remained hot at the same level since launch), but we want to be conservative here to ensure that these populations are calibrated correctly. Also, other potential strategies, such as only selecting pixels whose bad pixel values have changed since launch, miss some pixels with time-dependent dark current behaviors (e.g.

a pixel that has always been unstable, but at different levels). We omit modifying any pixels that have been consistently dead since launch, as these pixel populations do not show any time evolution and nearly all of these pixels are contained in the death star (a circular region near the bottom left edge of the detector) and the unbonded pixel regions along the top edge and top corners of the detector.

For each of the potentially time-dependent pixels specified above, we determine which cycles' data to combine together to generate its values in a given cycle's superdarks by looking at its behavior in the full-frame SPARS200 `FLT` darks from the internal WFC3/IR dark calibration programs; these darks have consistently been taken ∼every two weeks since launch and have long exposure times of 2803 s. Like for the full-stack superdark generation process, we omit any pixels with estimated persistence levels greater than ∼10% of the overall median dark current level or any darks exhibiting IR banding when making this determination. To determine which cycles' data to combine together to generate a given pixel's values in a given cycle's superdarks, we first calculate that pixel's robust mean and standard deviation, as well as its median and median absolute deviation (MAD; multiplied by 1.483 to make it similar to the standard deviation of a normal distribution) through the stack of calibration darks for each cycle. We next calculate the fraction of darks in each cycle whose values for that pixel are above a given cycle's (i.e. the cycle of interest's) robust mean or median for that pixel. Any cycles' measurements that meet the following criteria for a given pixel are combined together to generate that pixel's values in a given cycle's superdarks (note: measurements of the cycle of interest are designated by subscript i in the following equations):

1. The robust mean for the pixel through the cycle is within the robust mean of the pixel through the cycle of interest plus or minus two times the robust standard deviation of the pixel through the cycle of interest OR the median for the pixel through the cycle is within the median of the pixel through the cycle of interest plus or minus two times the MAD of the pixel through the cycle of interest.

$$\text{Mean}_i - 2\sigma_i \leq \text{Mean} \leq \text{Mean}_i + 2\sigma_i$$

$$\text{Median}_i - 2\text{MAD}_i \leq \text{Median} \leq \text{Median}_i + 2\text{MAD}_i$$

2. The robust standard deviation of the pixel through the cycle is greater than or equal to one half of the robust standard deviation of the pixel through the cycle of interest but less than or equal to two times the robust standard deviation of the pixel through the cycle of interest OR the MAD of the pixel through the cycle is greater than or equal to one half of the MAD of the pixel through the cycle of interest but less than or equal to two times the MAD of the pixel through the cycle of interest.

$$\frac{1}{2}\sigma_i \leq \sigma \leq 2\sigma_i$$

$$\frac{1}{2}\text{MAD}_i \leq MAD \leq 2\text{MAD}_i$$

3. At least 20% of the values for the pixel in the cycle are above or below the robust mean or median of the pixel through the cycle of interest.

We find that any cycle's data that meets the above criteria has a similar distribution in dark current values for a given pixel as the cycle of interest (i.e. the pixel's dark current behaviors are similar between the cycles). In using multiple metrics (e.g. mean and median) in each criterion, we catch any borderline similarities between the cycles in order to maximize the number of individual darks going into each measurement in the superdarks. We show examples of this process in Figure 3. Here, we show which cycles' data are combined together to generate a pixel's values in each cycle's superdarks after applying the above criteria.

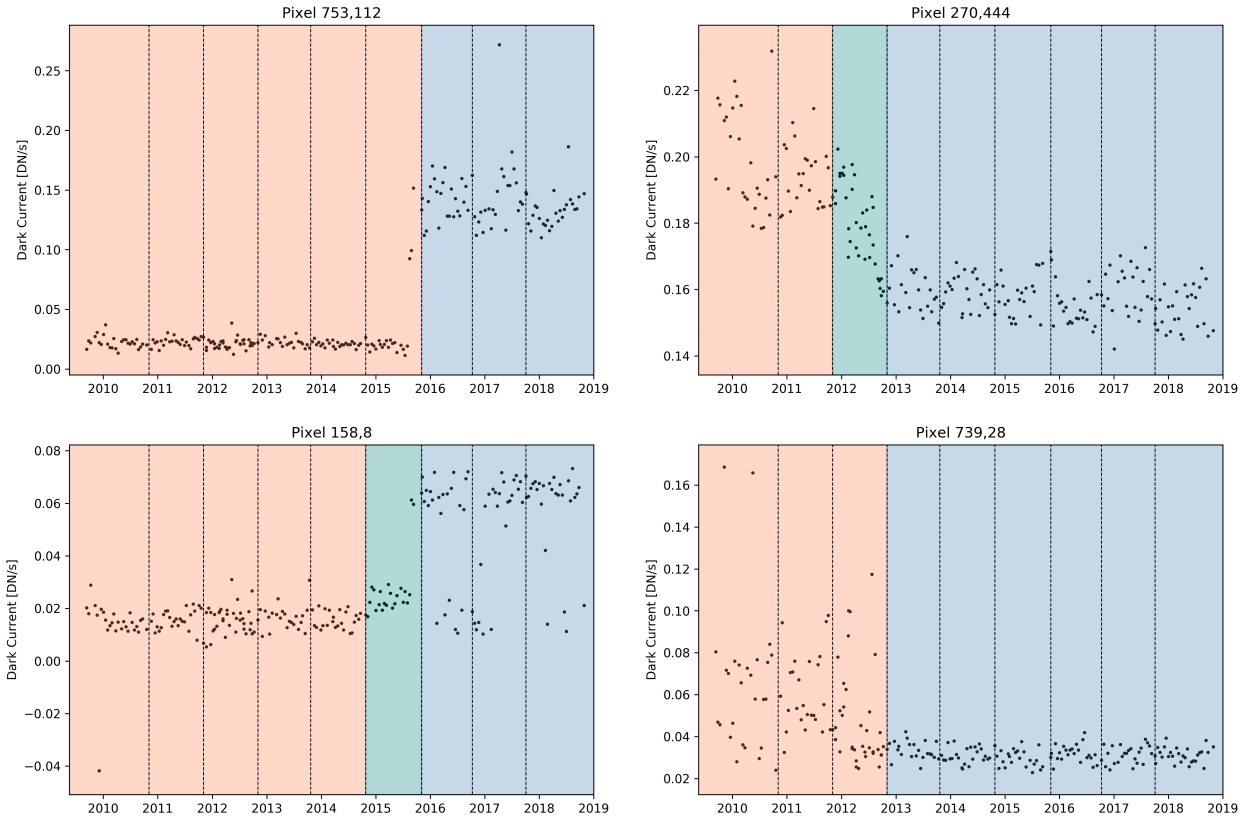

Figure 3: Examples of how each cycle's data are combined together to generate a pixel's values in each cycle's superdarks. The pixel countrates shown come from the full-frame SPARS200 `FLT` darks from the internal WFC3/IR dark calibration programs, and the vertical lines signify the USEAFTER times for each cycle's superdarks (see Table 2). As an example, the value of the pixel in the top left plot in the Cycle 17-22 superdarks is a combination of all of the Cycle 17-22 data (shaded in orange), and its value in the Cycle 23-25 superdarks is a combination of all of the Cycle 23-25 data (shaded in blue). These combinations were determined using the criteria listed in this section.

Once the determination is made on which cycles' data to consider when generating the superdark values for each time-dependent pixel, we follow the same combination process that was used to generate the full-stack superdark values described in Section 3.1; that is, we average all of the relevant cycles' `IMA` science data together using a 3-sigma robust mean for each read - ignoring those pixels flagged as either persistence or a cosmic ray hit. We also update the corresponding error values (the robust standard deviation of the values that went

into the science average divided by the square root of the number of values used) and sample values (the number of values used in the science and error calculations) in the same manner that was used in the full-stack superdark generation process for each read. We repeat this process for each time-dependent pixel to generate updated values in each cycle's superdarks.

Each cycle, we generate new superdarks using the process described above for each observing mode (but always using the full-frame SPARS200 `FLT` darks when determining which cycle's data to combine together, as these are the only observing mode to have been taken in a consistent cadence since launch). Because the number of darks observed in each observing mode varies through the dark calibration programs, the total number of darks used to generate a given time-dependent pixel's superdark values varies by the cycle and observing mode. For this reason, in the rare instances that a time-dependent pixel has less than five good values to combine together to generate its value in one of these superdarks, we default to the full-stack values that were calculated for this pixel in Section 3.1, and we flag this pixel as unstable in the superdark DQ extensions. This process only flags an additional ∼100 unstable pixels that aren't already included in the corresponding bad pixel tables from Sunnquist et al. (2019).

In Figure 4 we show examples of the results of this time-dependent modification process. The superdark values of the time-dependent pixels in these updated superdarks are much more accurate than the full-stack values that were used in the past (and described in Secition 3.1).

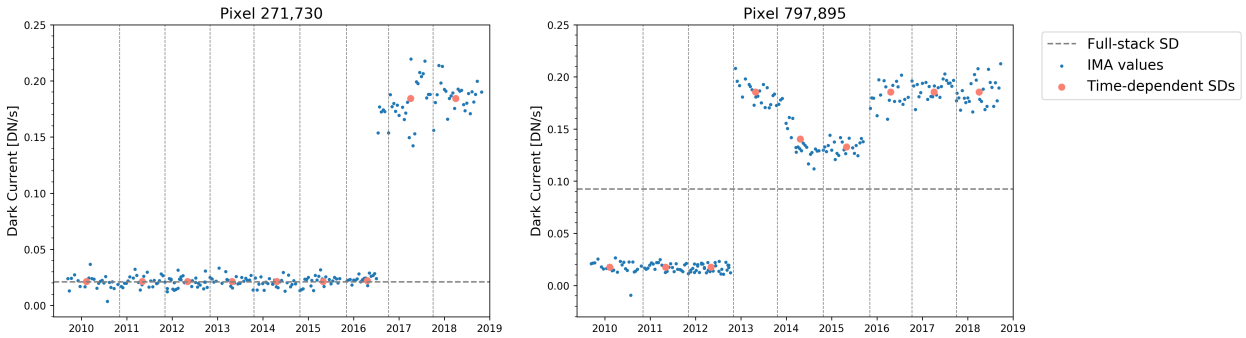

Figure 4: Pixel history of two pixels with the superdark values determined for each cycle over-plotted in orange. The pixel countrates shown come from the final read of the full-frame SPARS200 `IMA` darks from the internal WFC3/IR dark calibration programs, and the vertical lines signify the USEAFTER times for each cycle's superdarks (see Table 2). The superdark values for each cycle's full-frame SPARS200 superdark are shown in orange, and the horizontal line shows what the superdark value would have been had the full-stack superdark values from Section 3.1 been used. Clearly, the cycle-based superdark values are more representative of the time-dependent pixels' dark current behaviors, which justifies the use of the time-dependent modification process described in this section.

Finally, we again assure that these updated superdarks run successfully as a dark reference file through the `calwf3` calibration pipeline. We also perform a number of checks to make sure that the time-dependent pixel values in the updated superdarks are well-represented by the individual `IMA` files for each extension and every observing mode (e.g. Figure 4).

4 Analysis

One of the main improvements with these new time-dependent superdarks is the large increase in the number of input darks that went into their creation. From Table 1, we see that these new superdarks incorporate an average of 74 additional input darks (between 4 and 334 darks depending on the observing mode) than the previous superdarks. This increase corresponds to an average increase in exposure time of 527 minutes (between 1.7 to 4578 minutes depending on the observing mode). The large range in these values is due to the different exposure times of each observing mode and the varying number of darks observed in each observing mode in the dark calibration programs.

The large increase in the number of input files results in many statistical improvements in the new superdarks. For example, we find that the standard deviation of the science array values decreases by an average of 12% in the new superdarks compared to the previous superdarks (Table 3); the RAPID/512 superdark saw the greatest of these decreases at 34%. Due to the stability of the overall WFC3/IR dark current level (Sunnquist et al., 2017-04; Hilbert & Petro, 2012), the average science array values remain relatively unchanged. We find that the small increases or decreases in these average values are potentially induced by the HST orbital phases during the new individual dark exposures, which may not align with those from the older dark exposures (Sunnquist et al. (2017-24) found that the location of HST in its orbital day/night cycle affected the median WFC3/IR dark current levels). As was also noted in Dulude et al. (2014-06), many of the short subarray modes have negative mean superdark values; this is likely due to detector reset effects and read noise dominating the measured signals in these short exposures.

Table 3: Robust (3-sigma clipped) statistical comparison of the final read science arrays of the new Cycle 25 superdarks presented in this work to the previous superdarks they are replacing. Units are in counts.

Observing Mode		**Exposure**	**Mean**		**Median**		**Std Dev**	
Sample Sequence	**Aperture**	**Time**	**Old**	**New**	**Old**	**New**	**Old**	**New**
SPARS200	IR	2802.94	56.22	56.04	55.10	54.91	8.79	8.65
SPARS100	IR	1402.94	27.01	26.93	26.38	26.27	4.74	4.78
SPARS50	IR	702.94	13.30	13.22	12.99	12.89	2.89	2.91
SPARS25	IR	352.94	4.97	5.02	4.88	4.92	1.89	1.86
SPARS25	IRSUB512	321.75	3.49	3.57	3.46	3.54	2.40	2.19
SPARS25	IRSUB256	313.12	1.37	1.53	1.26	1.44	2.37	2.12
SPARS10	IR	142.95	0.83	1.06	0.82	1.05	1.59	1.39
SPARS10	IRSUB256	103.13	-2.23	-2.17	-2.23	-2.16	2.07	1.56
SPARS10	IRSUB128	100.65	-3.85	-3.62	-3.95	-3.72	2.30	2.07
SPARS5	IR	72.94	0.53	0.34	0.56	0.32	3.17	2.69
SPARS5	IRSUB512	41.75	-1.27	-1.45	-1.24	-1.42	2.86	1.96
SPARS5	IRSUB256	33.13	-2.71	-2.69	-2.68	-2.68	2.64	2.07
STEP400	IR	2799.24	55.79	55.00	54.69	53.89	9.75	8.88
STEP200	IR	1599.23	31.19	31.42	30.51	30.74	5.41	5.39
STEP100	IR	899.23	16.85	16.96	16.46	16.57	3.65	3.56
STEP50	IR	499.23	8.09	8.26	7.92	8.07	2.41	2.38
STEP25	IR	274.23	3.17	3.37	3.11	3.31	1.94	1.76

STEP25	IRSUB512	243.05	1.65	1.50	1.59	1.46	2.20	1.92
RAPID	IR	43.98	0.03	0.05	0.04	0.07	1.40	1.08
RAPID	IRSUB512	12.80	-0.62	-0.65	-0.59	-0.62	1.44	0.95
RAPID	IRSUB256	4.17	-0.64	-0.63	-0.58	-0.57	1.09	0.97
RAPID	IRSUB128	1.69	-0.71	-0.73	-0.62	-0.64	1.23	1.00
RAPID	IRSUB64	0.91	-1.20	-1.16	-1.14	-1.13	1.17	1.05

In Figure 5, we show the distribution of the final read science array values in the old and new full-frame SPARS200 superdark. These distributions look very similar, though the new superdark shows more pixels with high dark current values; this is likely due to the increase in the number of hot and unstable pixels noted in Sunnquist et al. (2019) since the creation of the old superdark.

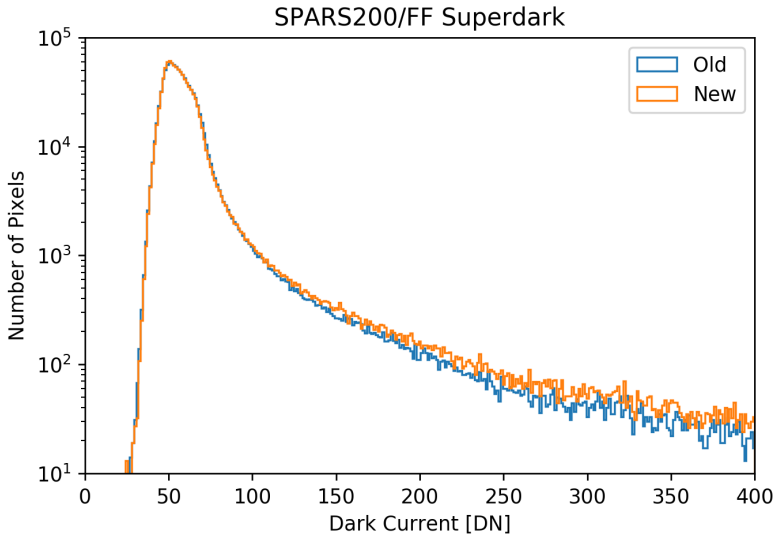

Figure 5: Distributions of the final read science array values in the new Cycle 25 SPARS200/FF superdark and the old SPARS200/FF superdark from Dulude et al. (2014-06).

These new superdarks also show many improvements in their error array values compared to the previous superdarks (Table 4). The average error array value decreases in every one of these new superdarks by between 9% and 67%, with an average decrease of 30%. The standard deviation of these error array values also decreases in every observing mode, with an average decrease of 48%.

Table 4: Robust (3-sigma clipped) statistical comparison of the final read error arrays of the new Cycle 25 superdarks presented in this work to the previous superdarks they are replacing. Units are in counts.

Observing Mode		**Exposure**	**Mean**		**Median**		**Std Dev**	
Sample Sequence	**Aperture**	**Time**	**Old**	**New**	**Old**	**New**	**Old**	**New**
SPARS200	IR	2802.94	2.02	1.04	2.02	1.04	0.26	0.08
SPARS100	IR	1402.94	0.82	0.75	0.82	0.75	0.05	0.04

SPARS50	IR	702.94	0.72	0.65	0.72	0.65	0.04	0.04
SPARS25	IR	352.94	0.86	0.73	0.86	0.73	0.06	0.05
SPARS25	IRSUB512	321.75	1.46	1.06	1.46	1.06	0.18	0.09
SPARS25	IRSUB256	313.12	1.33	0.86	1.33	0.86	0.15	0.06
SPARS10	IR	142.95	1.12	0.80	1.12	0.80	0.11	0.06
SPARS10	IRSUB256	103.13	1.41	0.47	1.41	0.47	0.17	0.02
SPARS10	IRSUB128	100.65	1.17	0.70	1.16	0.70	0.12	0.04
SPARS5	IR	72.94	2.76	2.38	2.77	2.38	0.83	0.56
SPARS5	IRSUB512	41.75	2.53	1.66	2.54	1.67	0.67	0.26
SPARS5	IRSUB256	33.13	2.20	1.60	2.21	1.60	0.47	0.24
STEP400	IR	2799.24	3.58	1.79	3.58	1.79	1.09	0.22
STEP200	IR	1599.23	1.10	0.91	1.10	0.91	0.09	0.06
STEP100	IR	899.23	1.23	0.99	1.23	0.99	0.12	0.08
STEP50	IR	499.23	0.99	0.84	0.99	0.84	0.08	0.06
STEP25	IR	274.23	1.20	0.87	1.20	0.87	0.12	0.06
STEP25	IRSUB512	243.05	1.46	1.05	1.46	1.05	0.18	0.09
RAPID	IR	43.98	1.18	0.78	1.18	0.77	0.12	0.05
RAPID	IRSUB512	12.80	1.27	0.65	1.27	0.65	0.14	0.04
RAPID	IRSUB256	4.17	0.78	0.61	0.78	0.61	0.05	0.03
RAPID	IRSUB128	1.69	0.92	0.57	0.91	0.57	0.07	0.03
RAPID	IRSUB64	0.91	0.63	0.48	0.72	0.55	0.26	0.20

In Figure 6, we show the distribution of the final read error array values in the old and new full-frame SPARS200 superdark. Here, we can see the lower peak value and reduced dispersion quantified in Table 4.

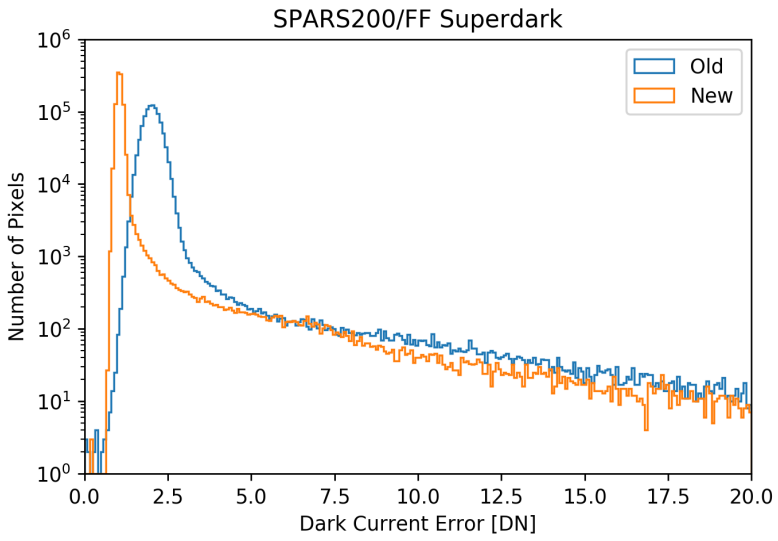

Figure 6: Distributions of the final read error array values in the new Cycle 25 SPARS200/FF superdark and the old SPARS200/FF superdark from Dulude et al. (2014-06). These error array values are significantly reduced in the new superdark.

To demonstrate the advantages of using these new superdarks as a reference file in the

`calwf3` pipeline, we calibrate an individual full-frame SPARS200 dark using both the old and new (Cycle 25) full-frame SPARS200 superdarks. As we show in Figure 7, this new superdark successfully calibrates thousands of additional time-dependent pixels that are not accounted for by the old superdark (e.g. pixels that have become hot or unstable or those that have returned to a normal state since launch), and the standard deviation of the calibrated dark is reduced by 76% using the new superdark. To help visualize these improvements, we show a 300x300 pixel cutout of these images in Figure 8. These results are not surprising, given that the old superdark only includes data through Cycle 20, and as Sunnquist et al. (2019) showed, thousands of pixels have changed their dark current behaviors since that time. The old superdark also combines all of the dark exposures together through time - disregarding any time-dependence shown in the pixels' dark current levels like those presented in Figure 4.

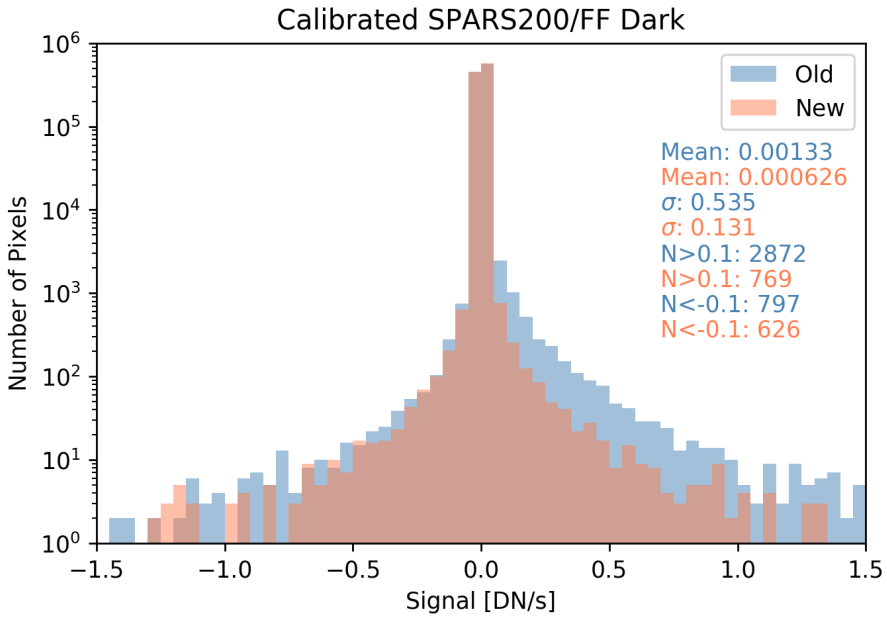

Figure 7: Distributions of a dark exposure calibrated using the old and new (Cycle 25) superdarks (a perfect calibration here would result in a distribution of all zeros). The new superdark calibrates thousands of additional time-dependent pixels not accounted for in the old superdark - both those that have become hot over time (contained in the upper tail of the old distribution) and those that have returned to a normal dark current level (contained in the lower tail of the old distribution). The overall remaining signal is similar after these two calibrations (due to the stability of the detector-wide dark current level), but the standard deviation of the calibrated dark is reduced by 76% using the new superdark (due to better calibration of the time-dependent pixels (e.g. Figure 4) and a large increase in the total number of input files used to generate the new superdark (Table 1)).

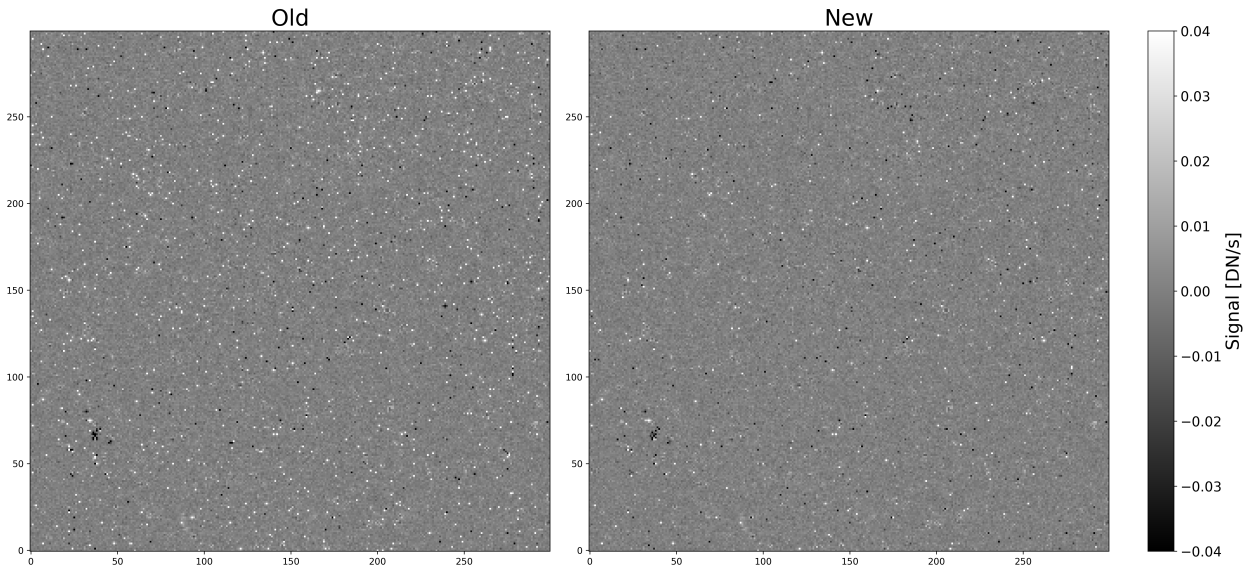

Figure 8: 300x300 pixel cutouts of the `FLT` images from Figure 7 that show how the calibration improves using the new superdark. The new superdark successfully calibrates many of the time-dependent hot and unstable pixels that are not accounted for in the old superdark. Pixels that still have large signal offsets after the new superdark calibration are likely unstable; while the new superdark provides more accurate values for these unstable pixels, their dark current levels still vary wildly from image to image.

5 Summary

Using data from internal dark calibration programs, we created new WFC3/IR superdarks for all observing modes offered to users. We incorporated an additional four years of dark data compared to the last time these superdarks were created (Dulude et al., 2014-06). This additional data significantly reduced the errors associated with the superdark values (Table 4).

Unlike previous superdark releases, we also updated the values of time-dependent pixels on a cycle-by-cycle basis - resulting in a new batch of superdarks delivered each cycle. This allows for better calibration of those ∼3.5% of detector pixels noted in Sunnquist et al. (2019) that have changed their dark current behaviors since launch (e.g. pixels that have become hot or unstable, or those that have returned to a normal state).

These new superdarks have been delivered and incorporated into the `calwf3` pipeline along with the new accompanying time-dependent WFC3/IR bad pixel tables (Sunnquist et al., 2019).

Recommendations

As of May 2019, the MAST processing pipeline flags stable and unstable hot pixels with different data quality values.

Observers who work directly with the `FLT`/`IMA` files can choose to reclaim the calibrated

stable hot pixels by NOT discarding pixels with DQ flag=16. We recommend continuing to treat unstable pixels (DQ flag=32) as bad.

Observers who work with drizzled data (drz files) should note that stable hot pixels (DQ flag=16) are by default reclaimed and treated as good pixels; pixels identified as unstable (flag=32) continue to be treated as bad. This change has been implemented in the pipeline via an updated AstroDrizzle parameter table (Mack & Bajaj, 2019) which is used in conjunction with the new pipeline darks (this ISR) and bad pixel tables (Sunnquist et al., 2019). The AstroDrizzle parameter table defines the recommended drizzling parameters for each instrument and can be used together with the new calibration reference files in order to recover stable hot pixels in drizzled images. For more information on modifications to the MDRIZTAB settings, please see Mack & Bajaj (2019).

Observers with archival data prior to May 2019 may re-request their data from the MAST portal to have their data automatically reprocessed and redrizzled with the new reference files.

References

Dulude, M.J., Baggett, S., Bushouse, H., and Hilbert, B., 2011. WFC3 ISR 2011-04. **"WFC3/IR Banding"**.

Dulude, M.J., Baggett, S., and Hilbert, B., 2014. WFC3 TIR 2014-02. **"WFC3/IR Dark Reference File Generation"**.

Dulude, M.J., Baggett, S., and Hilbert, B., 2014. WFC3 ISR 2014-06. **"New WFC3/IR Dark Calibration Files"**.

Hilbert, B., and Petro, L., 2012. WFC3 ISR 2012-11. **"WFC3/IR Dark Current Stability"**.

Long, K. S., Baggett, S., and MacKenty, J. W., 2015. WFC3 ISR 2015-15. **"Persistence in the WFC3 IR Detector: An Improved Model Incorporating the Effects of Exposure Time"**.

Mack, J., and Bajaj, V., 2019. WFC3 ISR 2019-05. **"Improved Drizzled Data Products for the WFC3/IR Detector"**.

Sunnquist, B., Baggett, S., Long, K.S., 2017. WFC3 ISR 2017-04. **"An Exploration of WFC3/IR Dark Current Variation"**.

Sunnquist, B., Baggett, S., Long, K.S., 2017. WFC3 ISR 2017-24. **"A Predictive WFC3/IR Dark Current Model"**.

Sunnquist, B., Brammer, G., Baggett, S., 2019. WFC3 ISR 2019-03. **"Time-dependent WFC3/IR Bad Pixel Tables"**.

Acknowledgments

The authors would like to thank Catherine Martlin for the review of this document and for providing many useful suggestions to improve its clarity. The authors would also like to thank Jennifer Mack, Heather Kurtz, Varun Bajaj & Nor Pirzkal for testing these new reference files and providing useful feedback.